23

Angular properties of refractive index sensor based on reflection interferometer

© V.S. Terentyev, V.A. Simonov

Institute of Automation and Electrometry, Siberian BranchRussian Academy of Sciences, Novosibirsk, Russia

e-mail: terentyev@iae.nsk.su

The angular properties of sensor, implemented in Kretschmann?s scheme, where the optimized for oblique incidence of light thin-film reflection interferometer acts as a sensing element, are described in the paper. Analytical equations, defining the sensor?s properties for S and P polarization states at working wavelength in vicinity of working angle of incidence, are provided, as well as approximate equations for main parameters of sensor: sensitivity, angular full width at half maximum, contrast and figure of merit. The possibility to vary the named parameters by choosing appropriate metal and dielectric layers of the structure is shown. For an example, the numerical calculations are made for one of special cases, optimized for S polarization state, as having larger figures of merit. The dependencies of angular properties on number of layers and base thickness are demonstrated. It is shown, that angular measurements with this method are theoretically capable of infinite figures of merit, and in practice they are only limited by losses in layered structure and beam divergency. The recommendations for experimental realization of method are given.

Keywords: reflection interferometer, total internal reflection, refractive index sensor.

1. Introduction

One of the most important parameters of any material medium is a refraction index, which in its turn may depend on temperature, pressure, humidity and presence of other chemical substances. Measurement of the refraction index, both absolute and relative, may provide valuable information about the medium state, which is actively used in chemistry and biology [1,2]. Currently there are many methods and optical schemes to determine the refraction index. These include methods with volume schemes like Kretschman configuration [3], fiber schemes [4,5], waveguide schemes based on microresonators [6] and diffraction schemes [7,8]. Each of these schemes has its advantages and disadvantages. For example, the advantage of fiber and waveguide schemes is in compact size of a sensitive element, ability of integration into other materials, high sensitivity. A disadvantage of fiber schemes is relatively large width of signal peaks and drops, which limits figure of merit (FOM) of such sensors. A disadvantage of microresonator schemes is lower sensitivity because- of comparatively long resonator bases (more than $10\,\mu m$), and inability to increase figure of merit because of - waveguide wall manufacturing defects, hard-to-get and costly technology of electron beam lithography. Diffraction schemes may have high figures of merit, and help to develop narrow signal spectral or angular minima with FOM $\sim 10^3-10^4$ [RIU^{-1}] (RIU — refractive index unit), but to make those, it is necessary to manufacture diffraction elements with submicron period by lithography methods.

The papers [9–11] investigated new structures of the sensitive layer in a classic Kretschman configuration based on metal-dielectric multi-layer coating using multi-beam interference. With the help of modelling it was shown that such structure could be made as a thin film version of a reflective interferometer (RI) with narrow spectral signal peaks and very high FOM, which may theoretically rise infinitely, and practically to more than 10^3 and is limited only by losses of light and drift of the beam in the structure layers. The advantage of this method consists in using a standard technology for sputtering thin interference layers and requires no other comparatively more complicated methods of photolithography or fiber optics. Besides, the advantage of spectral sensors based on thin metal films with a peak in reflection, called sensors with inverted plasmon resonance in the literature [12], may consist in additional increase of FOM by narrowing of a signal peak when used in the laser scheme.

The objective of this paper is to investigate the angular characteristics of the refraction index sensor based on the reflective interferometer in the Kretschman configuration for inclined light incidence, in the angular dependence of the refraction index of which there are narrow intensity peaks.

2. RI theory for inclined light incidence

The structure of the sensor shown in fig. 1 is fully identical to the structure of the spectral sensor [11]. It consists of
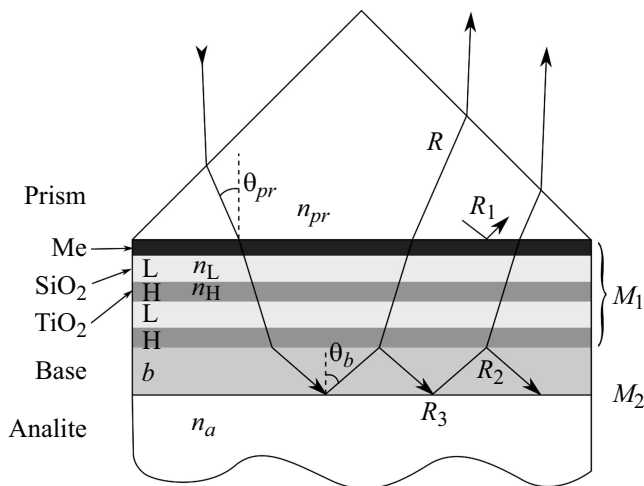
Figure 1. Optical scheme of the sensor based on inclined RI: Prism — prism (refraction index n_{pr}), Me — thin metal film, multilayer dielectric coating from material with high (H, n_H) and low (L, n_L) refraction indices, b, Base — base layer (n_b), a, Analyte — analyte (n_a), θ_{pr} — angle of incidence in prism, θ_b — angle of incidence in base layer, $R_{1,2}$ — mirror reflection indices M_1, R_3 — mirrors M_2.

a prisma with refraction index n_{pr}, the objective of which is to create the conditions for total internal reflection at the interface with analyte medium (Analyte), having refraction index n_a. A thin metal film is applied on the prism with thickness of much less than the wavelength, for example, titanium film 8 nm. Then dielectric layers are applied on the film with small n_L and large n_H ($n_L < n_H$) refraction indices, for example, TiO$_2$ and SiO$_2$, accordingly. Thickness of dielectric layers is selected so that whenever there is inclined incidence near the angle of total internal reflection (TIR) in prism $\theta_{\text{TIR}} = \arcsin(n_a/n_{pr})$ they are quarter-wave, i.e. their thickness is $h_j = \lambda_w/(4n_j \cos\theta_j^w)$, $j = L, H$, $\cos\theta_j^w = \sqrt{1 - (n_{pr}\sin\theta_{pr}^w/n_j)^2}$, $Im(\cos\theta_j^w) \leq 0$, θ_j^{pr} — „working" angle of incidence and λ_w — light wavelength in the sensor. Dielectric layers form a front mirror M_1 of the reflective interferometer. Then there is a base layer, which borders with analyte. Thickness of the base layer is such that at least one maximum is formed in reflection from such structure. In the base layer under resonant conditions the field maximum is concentrated, i.e. multibeam interference takes place. The back mirror M_2 is the interface between the base and the analyte. Under TIR the energy coefficient of reflection from the border of the base and the analyte is very close to one, and whenever the analyte refraction index changes, only the mirror reflection phase changes M_2.

If $\Psi_{1,2}$, Φ_1 are known— phases of reflection and transmission coefficients, accordingly $R_{1,2}$ and transmission $T_1 = T_2$ of mirror M_1, Ψ_3 — phase and coefficient of reflection R_3 of back mirror M_2, the energy coefficient of

reflection $R(\varphi)$ of RI is described by formula [13–15]:

$$R(\varphi) = R_1 + 2T_1\sqrt{R_1R_3}\frac{\cos(\vartheta + 2\varphi) - \sqrt{R_1R_3}\cos(\vartheta)}{1 + R_2R_3 - 2\cos(2\varphi)\sqrt{R_2R_3}}$$

$$+ \frac{R_3T_1^2}{1 + R_2R_3 - 2\cos(2\varphi)\sqrt{R_2R_3}}, \tag{1}$$

$$\vartheta = \Psi_1 + \Psi_2 - 2\Phi_1 \text{ [rad]},$$

$$\varphi(\theta_{pr}, \lambda) = \frac{2\pi n_b h_b \cos\theta_b(\theta_{pr})}{\lambda}$$

$$- \frac{\Psi_2(\theta_b(\theta_{pr}), \lambda) + \Psi_3(\theta_b(\theta_{pr}), \lambda)}{2} \text{ [rad]}, \tag{2}$$

where λ — wavelength, θ_b — angle of light incidence on mirrors inside the resonator, i.e. in the base layer, besides, this angle is the function of the angle of incidence in the prism $\theta_b(\theta_{pr})$, h_b — thickness, n_b — RI base refraction index, $R(\varphi)$ is fair for S- and P-polarizations with substitution of corresponding coefficients $R_{1,2,3}$, T_1 and their phases for this polarizations. Phase progression between mirrors $\varphi(\theta_{pr}, \lambda)$ in the general case is the function of the angle of incidence and wavelength, and also the refraction index of analyte n_a.

3. Analytical formulae for front mirror coefficients

For dielectric layers of quarter-wave thickness of the mirror M_1 in the amount of N two-layer units comprising layers with low (L) and high (H) refraction indices, expressions may be written for energy reflection and transmission coefficients at working wavelength λ_w [11]:

$$R_1^{[S,P]} = \frac{\left(u_{pr} - \xi_1 - u_b(u_L/u_H)^{2H}\right)^2 + \xi_2^2}{\left(u_{pr} + \xi_1 + u_b(u_L/u_H)^{2H}\right)^2 + \xi_2^2}, \tag{3}$$

$$\text{tg}\,\Psi_1^{[S,P]} = \frac{2u_{pr}\xi_2}{\left(\xi_1 + (u_L/u_H)^{2N}u_b\right)^2 - u_{pr}^2 + \xi_2^2}, \tag{4}$$

$$R_2^{[S,P]} = \frac{\left(u_{pr} + \xi_1 - u_b(u_L/u_H)^{2H}\right)^2 + \xi_2^2}{\left(u_{pr} + \xi_1 + u_b(u_L/u_H)^{2H}\right)^2 + \xi_2^2}, \tag{5}$$

$$R_2^{[S,P]} \approx 1 - \frac{4(u_{pr} + \xi_1)u_b}{(u_{pr} + \xi_1)^2 + \xi_2^2}\left(\frac{u_L}{u_H}\right)^{2N} + O\left(\left(\frac{u_L}{u_H}\right)^{4N}\right),$$

$$u_L < u_H,$$

$$\text{tg}\,\Psi_2^{[S,P]} = \frac{2(u_L/u_H)^{2N}u_{pr}\xi_2}{(u_{pr} + \xi_1)^2 - (u_L/u_H)^{4H}u_b^2 + \xi_2^2}, \tag{6}$$

$$T_1^{[S,P]} = T_2^{[S,P]} = \frac{4(u_L/u_H)^{2H}u_{pr}u_b}{\left(u_{pr} + \xi_1 - u_b(u_L/u_H)^{2H}\right)^2 + \xi_2^2}, \tag{7}$$

where u_j ($j = L, H, pr, b$), and ξ must be substituted for the corresponding polarizations:

$$u_j = \begin{cases} u_j^{[S]} = n_j\cos\theta_j & (S \text{ polarization}), \\ u_j^{[P]} = n_j/\cos\theta_j & (P \text{ polarization}), \end{cases}$$

$$\cos\theta_j = \sqrt{1 - (n_{pr}\sin\theta_{pr}/n_j)^2}, \quad \mathrm{Im}(\cos\theta_j) \le 0, \quad \text{and}$$

$$\xi^{[S]} = \xi_1^{[S]} + i\xi_2^{[S]} = 2k_0 h_m n_m \chi_m$$

$$+ i k_0 h\left((n_m^2 - \chi_m^2) - n_{pr}^2\sin^2\theta_{pr}\right),$$

$$\xi^{[P]} = \xi_1^{[P]} + i\xi_2^{[P]} = 2k_0 h_m n_m \chi_m + i k_0 h(n_m^2 - \chi_m^2), \quad (8)$$

n_m, χ_m — reflection and absorption index of the metal film, accordingly. Formulae $(3)-(8)$ are the generalization of similar formulae for normal incidence given in [13].

For the mirror M_2 one may write reflection phases for two polarizations:

$$\mathrm{tg}\,\Psi_3^{[P]} = \frac{2n_a^2 n_b^2\sqrt{f_b}\sqrt{f_a}}{n_a^4 f_b - n_b^4 f_a},$$

$$\mathrm{tg}\,\Psi_3^{[S]} = \frac{2\sqrt{f_b}\sqrt{f_a}}{f_b - f_a}, \quad (9)$$

where
$$f_a = \left(n_{pr}\sin(\theta_{pr})\right)^2 - n_a^2,$$
$f_b = n_b^2 - \left(n_{pr}\sin(\theta_{pr})\right)^2 - n_a^2$.

If metal film parameters are specially agreed, i.e. $\xi_1 = u_{pr}$ is provided by selecting film thickness h_m, and metal is selected with $n_m \approx \chi_m$, then from (3) and (8) it follows that $R_1 \ll 1$, and from (5) — $R_2 \to 1$ with the growth of the number of dielectric two-layer units N. This creates mirror M_1 that is asymmetric by reflection coefficients. Then responce function R in the reflection will be similar to hardware function of Fabry−Perot interferometer in transmission, i.e. will have narrow maxima of intensity (in formula (1) the first two members will become negligibly small).

4. Main sensor characteristics

To assess the main characteristics of the sensor, it is necessary to determine the dependence of phase progression $\varphi(\theta_{pr})$ in the base layer measured for certainty in radians [rad], on angle of incidence θ_{pr}, measured in degrees [deg]. Variation of phase progression causes shift of RI resonant maxima position. If one suggests that the sensor is designed for the working angle θ_{pr}^w, then shift of the angular characteristic of reflection in this point will be inversely proportional to the derivative of the phase by angle of incidence $\left[\frac{\partial\varphi}{\partial\theta_{pr}}\right]^{-1}_{\theta_{pr}=\theta_{pr}^w}$. The inverse derivative defines the linear shift of the maximum by $\Delta\theta_{pr}$ to the position of the reflection maximum of the next longitudinal mode at variation of φ by π, which is an analog of equal inclination bands or shift by one area of free dispersion along the wavelength. However, the expression for the inverse derivative will be much more complicated for the angular sensor than for the spectral one, where partial derivative by wavelength may only be taken from the first member (2), if dispersion dependence of substance refraction indices is excluded. From phase expressions (2), (6), (9) it follows

that for multi-layer coating the reverse derivative is not linear on the base thickness h_b as well. Besides, it varies non-linearly at other angles of incidence $\theta_{pr} \ne \theta_{pr}^w$, even though it is not described by the above expressions already, accordingly, the sensitivity of the angular maximum position to the phase progression varies. Based on the above

$$\Delta\theta_{pr} \approx \pi\left[\frac{\partial\varphi}{\partial\theta_{pr}}\right]^{-1} \ [\text{deg}]. \quad (10)$$

Formula (10) is valid for the angles that are very different from θ_{pr}^w as well. The inverse derivative must be determined in numerical form, since even for angle θ_{pr}^w it was not possible to obtain a simple analytical expression for it. Taking into account (10), angular sensitivities of sensor $S_\theta^{[S,P]}$ may be expressed similarly [10], considering the derivative of the reflection phase of mirror M_2 to n_a:

$$S_\theta^{[S,P]} \approx \frac{\Delta\theta_{pr}}{\pi}\frac{\partial\varphi^{[S,P]}}{\partial n_a} \left[\frac{\text{deg}}{\text{RIU}}\right], \quad (11)$$

$$S_\theta^{[S]} \approx -\frac{\Delta\theta_{pr}}{2\pi}\frac{\partial\Psi_3^{[S]}}{\partial n_a} = \frac{\Delta\theta_{pr}}{\pi}\frac{n_a\sqrt{f_b}}{n_b^2 - n_a^2}\frac{1}{\sqrt{f_a}} \left[\frac{\text{deg}}{\text{RIU}}\right], \quad (12)$$

$$S_\theta^{[P]} \approx -\frac{\Delta\theta_{pr}}{2\pi}\frac{\partial\Psi_8^{[P]}}{\partial n_a} = \frac{\Delta\theta_{pr}}{\pi}\frac{n_b^2 n_a\sqrt{f_b}}{(n_a^4 f_b + n_b^4 f_a)}\frac{1}{\sqrt{f_a}} \left[\frac{\text{deg}}{\text{RIU}}\right], \quad (13)$$

where the last fraction in the products may rise infinitely with approximation of $\theta_{pr} \to \theta_{TIR}$.

Angular width $\delta\theta_{pr}^{[S,P]}$ at half-height of intensity maxima is related to $\Delta\theta_{pr}$ by ratio

$$\delta\theta_{pr}^{[S,P]} \approx \frac{\Delta\theta_{pr}}{F^{[P,S]}} \ [\text{nm}], \quad (14)$$

where $F^{[P,S]}$ — finesse of bands determining effective quantity of interfering beams:

$$F^{[P,S]} \approx \pi\frac{\sqrt[4]{R_2 R_3}}{1 - \sqrt{R_2 R_3}},$$

$$F^{[P,S]} \approx \pi\frac{(u_{pr} + \xi_1)^2 + \xi_2^2}{2(u_{pt} + \xi_1)u_b}\left(\frac{u_H}{u_L}\right)^{2N}, \quad u_L < u_H, \quad (15)$$

where $R_{2,3}$, $u_{pr,L,H,b}$, ξ_2 are taken for the corresponding polarizations. Theoretically F may continuously rise with increase N, and practically it is limited to losses only in the structure of the interferometer and beam drift.

For contrast of $C_\theta^{[S,P]}$ spectral characteristic, which directly influences sensor FOM, from theory of RI [13] one may write a precise formula, however in our case only a small region is of interest near the peak. Then, taking into account the fact that maximum coefficient of reflection is very close to one, and the minimum one has the value of the background determined by reflection coefficient R_1:

$$C_\theta^{[S,P]} \approx 1 - R_1^{[S,P]}. \quad (16)$$

This estimate provides smaller contrast values compared to precise RI formula, since it excludes potential minima at a large distance from the peak.

The formula to estimate FOM is produced from $(12)-(16)$:

$$\text{FOM}_\theta = C_\theta \frac{S_\theta}{\delta\theta} = C_\theta \frac{\Delta\theta_{pr}}{\pi\delta\theta} \frac{d\varphi}{dn_a} = C_\theta \frac{F}{\pi} \frac{d\varphi}{dn_a}. \quad (17)$$

With equal contrasts, FOMs by angle and wavelength are equal to $\text{FOM}_\theta = \text{FOM}_\lambda$ [10], they are determined only by parameters of mirrors and base layer and are not related to selection of the measurement method (by angle or wavelength).

Formulae $(10)-(17)$ may be used to estimate sensor parameters near θ_{pr}^w and λ_w. However, the more precise accounting of reflection phases, errors in the thickness of layers and base may shift the angular position of the maximum from the suggested one. Besides, numerical study of sensor characteristics is of interest at large angles, compared to θ_{pr}^w, since the analytical method of study for such angles is quite complicated in connection with complication of formulae $(3)-(7)$ type.

5. Numerical modeling of sensor characteristics

As an example, one may consider numerical modelling of the structure consisting of the film of titanium and dielectrics of titanium oxide and silicon oxide. This structure is similar to [11] and is optimized for S-polarization. Structure of layers: [Prism, Ti, $(L, H)^N$, B, Analyte], where N — number of two-layer units, Ti — titanium film, L — dielectric with low, H — with high refraction index, B — base layer, $h_{Ti} = 8\,\text{nm}$, $h_L = \lambda_w/(4n_L \cos\theta_L)$, $h_H = \lambda_w/(4n_H \cos\theta_H)$, $n_{Ti} = 3.68 - 4.61i$@1550 nm, $n_L = 1.46$ (SiO$_2$), $n_H = 2.4$ (TiO$_2$), $n_b = n_H$, $\lambda_w = 1550\,\text{nm}$. Thickness of titanium film was selected from the matching condition $\xi_1^{[S]} = n_{pr} \cos\theta_{pr}^w = 1.1$ ($n_{pr} = 1.52$, $\xi_2^{[S]} = -0.25$), for the working angle of incidence in the prism $\theta_{pr}^w = 43°$, close to angle of TIR ($\theta_{\text{TIR}} = 41.14°$, $n_a = 1$). The calculation was made by the method of characteristic matrices for layered media.

At fixed wavelength the important parameters are the angle of incidence in the prism θ_{pr}, number of two-layer units N and thickness of base layer h_b. Let us consider the dependence of the first parameter. According to (1), sensor properties may be written as separate parameters $R_1^{[S]}$, $R_2^{[S]}$ of the mirror M_1. Fig. 2 builds their dependences on the angle of incidence θ_{pr} for the above structure of layers and practically important $N = 3, 4, 5, 6$. Reflection coefficient $R_1^{[S]}$ weakly depends on N, therefore curves practically merge (fig. 2, a). It has low value near TIR angle (θ_{TIR}) according to formula (3), and as θ_{pr} increases, it tends to one, which, as evident from (16), causes
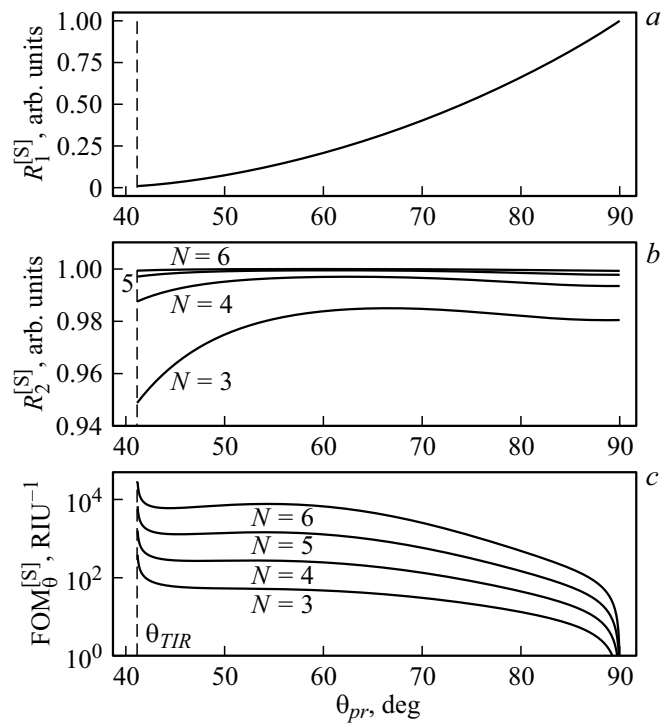

Figure 2. Dependences of reflection coefficients $R_1^{[S]}$ (a), $R_2^{[S]}$ (b), figure of merit $\text{FOM}_\theta^{[S]}$ (c) on the angle of incidence θ_{pr} for different N (in fig. (a) the curves merge).

deterioration of contrast (reduction of $C_\theta^{[S]}$) and reduction of FOM_θ. Reflection coefficient $R_2^{[S]}$ stronger depends on N, its value increases at growth of θ_{pr}, and becomes closer to the unit, in respect to angles close to θ_{TIR} (fig. 2, b). According to formulae (15), (17), with growth of $R_2^{[S]}$, FOM_θ increases. Therefore, first it seems to make more sense to locate the signal peak near the maximum of angular dependence $R_2^{[S]}$. However, calculation according to formula (17) shows (fig. 2, c), that from the point of view of high FOMs it makes more sense to operate in the region of angles close to θ_{TIR}. As it follows from the figure, for this system one may get FOMs above 10^4. However, at the same time as at large ranges of variation n_a the peak shift will occur with large non-linearity. If high linearity of peak shift is required, one may operate in the region of local maximum FOM_θ at angles near $50-60°$.

Parameters given in fig. 2 are identical for any lengths of bases h_b. For illustration purposes one may build angular distribution of intensity at reflection from the interferometer at minimum length of the base $h_b = h_H$ and $N = 3$, when there is only one signal peak located near TIR angle (fig. 3, a). The signal peak will narrow with increasing N, as shown in fig. 3, b. Varying h_b, one may move the peak to the required angle, for example, at $h_b = 1.5h_H$ the peak moves to the angle $\approx 55.6°$. If analyte refraction index changes by $\Delta n_a = 0.01$, this will cause angular shift of signal peak position by $0.36°$ (dotted line in fig. 3, a, b), which corresponds to angular sensitivity 36 [deg/RIU].
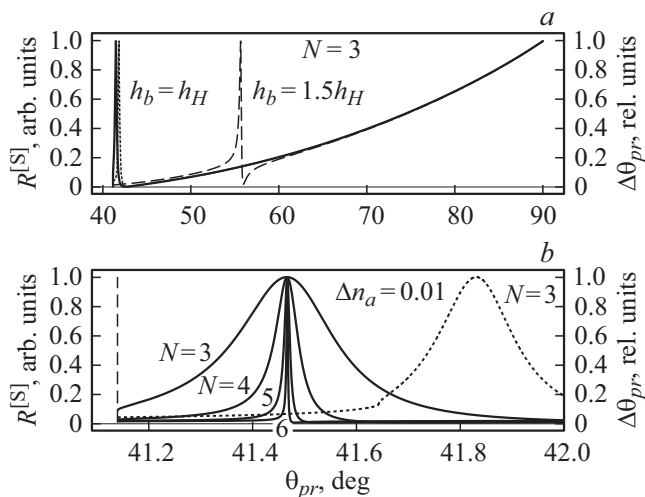
Figure 3. Dependences of reflection coefficient $R^{[S]}$ at $h_b = h_H$ and different N (solid lines) and shift by angle at $\Delta n_a = 0.01$ RIU (dotted line), at $h_b = 1.5h_H$ (dotted line) on angle of incidence θ_{pr} in the wide range of angles (a) and near TIR angle (b).

Base length h_b influences angular sensitivity of peak shift according to (10), in other words, dependence of phase progression (2) on angle θ_{pr} may be varied, as the number of peaks in the range of angles from θ_{TIR} to $90°$. Fig. 4, a shows the difference of phase progression $\Delta\varphi = \varphi(\theta_{pr}) - \varphi_{\min}$, where $\varphi_{\min}$ — minimum value of the phase in the specified angle limits, for two $h_b = 11h_H$, $51h_H$, in order to demonstrate several signal peaks within the angular characteristic. It is possible when $\Delta\varphi$ varies by more than π. Curve 1 in fig. 4, a has two crossings with integer values π, which corresponds to two maxima in fig. 4, b, curve 2 has 5 crossings, which corresponds to five maxima in fig. 4, c. As base length increases, angular sensitivity of the sensor drops, since inverse derivative is reduced in (10).

6. About experimental realization of the method

For angular measurements, the wavelength of sensor operation must be fixed $\lambda = \lambda_w$, but it is quite possible to operate in its small region $\lambda_w \pm \delta\lambda$, where sensor properties do not vary much. The smaller the width of the spectrum of radiation source, the narrower the limit signal maximum of reflection by angle may be. In the angular measurement scheme it is possible to precisely the source wavelength in small ranges and thus adapt the reflection peak for the necessary angle, precisely bringing it closer or further from TRI angle, thus changing angular sensitivity. For this purpose one may use a fiber laser with distributed feedback, having the smallest width of generation spectrum ($< 100\,\mathrm{kHz}$), rebuilt (including cyclically) by a piezoceramic and/or mechanical actuator, which potentially makes it possible to use one photodetector instead of the matrix.

Radiation may not be transmitted to the prism by convergent or divergent beam, generated by a cylindrical lens as one in the options of measurement schemes. Such spatial distribution may be unsuitable for multi-beam interference, if one takes into account continuous beam drift in the structure at each reflection because of inclined incidence, and with higher quantity of interfering beams it is possible to terminate interference because of absence of incident radiation at the necessary angle. The optimal would be the goniophotometer scheme, where radiation hits the structure being always collimated, where it is possible to vary the beam diameter, since the more the diameter, the more interfering beams may be produced.

7. Conclusion

The paper investigated angular characteristics of the sensor made in Kretschman configuration, where the sensitive element is the structure in the form of a thin-film version of the reflection interferometer, optimized for inclined incidence of light. Kretschman configuration is a one, which leads to advantages, including the possibility of implementation using the available technology, and disadvantages as well: susceptibility to vibrations and other external parasite exposures, impossibility of miniaturization. Therefore, development of the method of reflective interferometer as the sensor in integral and optical design may be the purpose of future research.

To describe sensor characteristics, analytical formulae are given for S- and P-polarizations at working wavelength λ_w and near the working angle of the sensor θ_{pr}^w, and also formulae that approximately describe the main character-
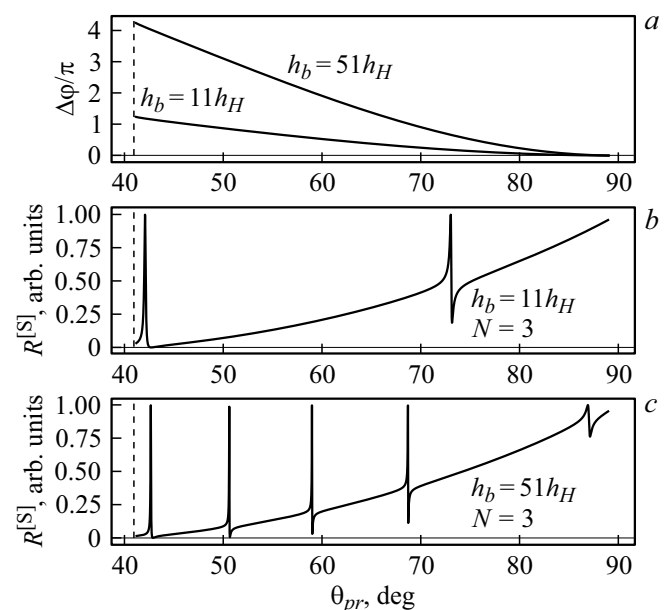

Figure 4. Dependences of difference in phase progression $\Delta\varphi/\pi$ for various thicknesses h_b (a), reflection coefficient $R^{[S]}$ at $h_b = 11\,h_H$ (b), $h_b = 51\,h_H$ (c) on angle of incidence θ_{pr}.

istics of the sensor: sensitivity $S_\theta^{[S,P]}$, angular width of the peak at half-height $\delta\theta_{pr}^{[S,P]}$, contrast $C_\theta^{[S]}$ and figure of merit $\mathrm{FOM}_\theta^{[S,P]}$. The possibility to vary the specified characteristics is shown by the corresponding selection of metal and dielectric layers of the structure, which sets this method apart, since variation may be carried out within widest limits.

As an example, numerical calculation is given for the characteristics of one special case of the sensor optimized for S-polarization as having the highest figures of merit. Angular properties of this sensor are demonstrated depending on the number of dielectric layers and size of the base. It was shown that this method may be used to produce very high figures of merit ($> 10^4$) at angular measurements. Recommendations are given on experimental realization of the method.

As shown in paper [9], when a non-quarter-wave dielectric layer is added between the metal film and the first dielectric layer, one may get minima with comparable width at half-height instead of intensity maximum in the reflection from the sensor. If sensor integration into the laser resonator is not provided for, it makes more sense from the point of view of signal/noise ratio to operate with the minimum rather than with the maximum. Main angular characteristics of such sensor are also described through the above formulae.

Funding

Conflict of interest

The authors declare that they have no conflict of interest.

References

[1] *Homola J.* Surface Plasmon Resonance Based Sensors, Springer, 2006.
[2] *Kooyman R.P.H., Schasfoort R.B.M., Tudos A.J.* Handbook of Surface Plasmon Resonance (2nd ed.), London: RSC, 2008.
[3] *Sadrolhosseini A.R., Shafie S., Soleimani H., Mahdi M.A.* // Optics & Laser Technology. 2021. V. 140. P. 106970. doi 10.1016/j.optlastec.2021.106970
[4] *Li C., Gao J., Shafi M., Liu R., Zha Z., Feng D., Liu M., Du X., Yue W., Jiang S.* // Photon. Res. 2021. V. 9. N 3. P. 379−388. doi 10.1364/PRJ.416815
[5] *Liu Q., Jiang Y., Sun Y., Hu C., Sun J., Liu C., Lv J., Zhao J., Yi Z., Chu P.K.* // Appl. Opt. 2021. V. 60. N 6. P. 1761−1766. doi 10.1364/AO.419518
[6] *Cardenosa-Rubio M.C., Robison H.M., Bailey R.C.* // Current Opinion in Environmental Science & Health. 2019. V. 10. P. 38−46. doi 10.1016/j.coesh.2019.09.001
[7] *Hlubina P., Urbancova P., Pudis D., Goraus M., Jandura D., Ciprian D.* // Opt. Lett. 2019. V. 44. N 22. P. 5602. doi 10.1364/OL.44.005602
[8] *Rahimi L., Askari A.A.* // Appl. Opt. 2020. V. 59. N 34. P. 10980. doi 10.1364/AO.405129
[9] *Goldina N.D.* // Avtometriya. 2021. V. 57. № 2. P. 122. (in Russian). doi 10.15372/AUT20210214
[10] *Terentiev V.S., Simonov V.A.* // Opt. i spektr. 2021. T. 129. № 2. P. 238. (in Russian) doi 10.21883/OS.2021.02.50564.232-20
[11] *Terentiev V.S., Simonov V.A.* // Opt. i spektr. 2021. T. 129. № 8. P. 1089. (in Russian). doi 10.21883/OS.2021.08.51207.1932-21
[12] *Printz M., Sambles J.R.* // J. Mod. Opt. 1993. V. 40. N 11. P. 2095. doi 10.1080/09500349314552131
[13] *Troitskiy Yu.V.* Mnogoluchevye interferometry otrazhennogo sveta. Novosibirsk: Nauka, 1985. 208 p. (in Russian).
[14] *Holden J.* // Proc. Phys. Soc. B. 1949. V. 62. N 7. P. 405. doi 10.1088/0370-1301/62/7/301
[15] *Simonov V.A.* // Novosibirsk: IAiE SO RAN, 2018. 99 p. (in Russian). https://www.iae.nsk.su/ru/dissertation-council/2458-dc-181226